Chemical Science

ROYAL SOCIETY OF CHEMISTRY

EDGE ARTICLE

View Article Online
View Journal | View Issue

Cite this: *Chem. Sci.*, 2022, **13**, 4070

All publication charges for this article have been paid for by the Royal Society of Chemistry

Pt(II)-coordinated tricomponent self-assemblies of tetrapyridyl porphyrin and dicarboxylate ligands: are they 3D prisms or 2D bow-ties?†

Paola A. Benavides,[a] Monica A. Gordillo,[a] Ashok Yadav,[a] M. Andrey Joaqui-Joaqui[b] and Sourav Saha*[a]

Thermodynamically favored simultaneous coordination of Pt(II) corners with aza- and carboxylate ligands yields tricomponent coordination complexes with sophisticated structures and functions, which require careful structural characterization to paint accurate depiction of their structure–function relationships. Previous reports claimed that heteroleptic coordination of *cis*-$(Et_3P)_2Pt^{II}$ with tetrapyridyl porphyrins (M′TPP, M′ = Zn or H_2) and dicarboxylate ligands (XDC) yielded 3D tetragonal prisms containing two horizontal M′TPP faces and four vertical XDC pillars connected by eight Pt(II) corners, even though such structures were not supported by their ^{1}H NMR data. Through extensive X-ray crystallographic and NMR studies, herein, we demonstrate that self-assembly of *cis*-$(Et_3P)_2Pt^{II}$, M′TPP, and four different XDC linkers having varied lengths and rigidities actually yields bow-tie (⋈)-shaped 2D $[\{cis\text{-}(Et_3P)_2Pt\}_4(M'TPP)(XDC)_2]^{4+}$ complexes featuring a M′TPP core and two parallel XDC linkers connected by four heteroleptic Pt^{II} corners instead of 3D prisms. This happened because (i) irrespective of their length (~7–11 Å) and rigidity, the XDC linkers intramolecularly bridged two adjacent pyridyl-N atoms of a M′TPP core *via* Pt^{II} corners instead of connecting two cofacial M′TPP ligands and (ii) bow-tie complexes are entropically favored over prisms. The electron-rich ZnTPP core of a representative bow-tie complex selectively formed a charge-transfer complex with highly π-acidic 1,4,5,8,9,12-hexaazatriphenylene-2,3,6,7,10,11-heaxacarbonitrile but not with a π-donor such as pyrene. Thus, this work not only produced novel M′TPP-based bow-tie complexes and demonstrated their selective π-acid recognition capability, but also underscored the importance of proper structural characterization of supramolecular assemblies to ensure accurate depiction of their structure–property relationships.

Received 23rd November 2021
Accepted 22nd February 2022

DOI: 10.1039/d1sc06533e

rsc.li/chemical-science

Introduction

Owing to the dynamic, directional, and self-selecting/rectifying nature of metal–ligand coordination bonds, metal-driven self-assembly processes have emerged as one of the most attractive and powerful tools of supramolecular chemistry, yielding myriads of supramolecular coordination complexes (SCCs) ranging from discrete metallacycles[1–10] and cages[11–23] to extended coordination polymers and metal–organic frameworks[24–26] over several decades. To obtain the target SCCs and to avoid statistical mixtures of different possibilities, only one rigid organic ligand is combined with a metal ion at an appropriate stoichiometry, which usually yields bicomponent coordination complexes. However, the resulting bicomponent SCCs often lack the structural and functional diversity and tunability needed for various advanced applications. Expanding the scope of coordination-driven self-assembly strategies, recently researchers have discovered[26–56] that *cis*-capped Pt(II) and Pd(II) corners simultaneously bind a carboxylate and a pyridyl ligand, which preferentially yield thermodynamically favored heteroleptic Pt(N,O) complexes instead of two different homoleptic complexes.[29–34,47–53] Furthermore, when two different homoleptic $Pt^{II}(COO^-)_2$ and $Pt^{II}(pyridyl)_2$ complexes were mixed together at an appropriate stoichiometry, they spontaneously reorganized into thermodynamically more stable heteroleptic Pt(N,O) complexes.[30,32,33] These revelations paved the way for metal-driven self-assembly of tricomponent metallacycles and cages containing two complementary ligands that could further diversify their structures, compositions, properties, and functions.

While it is fairly straightforward to assemble 2 : 2 : 4 tricomponent rectangles[30,32,41] having two parallel dicarboxylate and two parallel dipyridyl arms connected by four heteroligated $Pt^{II}(N,O)$ corners, the formation of 2 : 4 : 8 tricomponent tetragonal prisms featuring two cofacial tetratopic (tetrapyridyl

[a]*Department of Chemistry, Clemson University, Clemson, South Carolina 29634, USA. E-mail: souravs@clemson.edu*

[b]*Department of Chemistry, University of Minnesota, Minneapolis, MN 55455, USA*

† Electronic supplementary information (ESI) available. CCDC 2081606–2081610. For ESI and crystallographic data in CIF or other electronic format see DOI: 10.1039/d1sc06533e

or tetracarboxylate) ligands and four complementary ditopic (dicarboxylate or dipyridyl) linkers requires the latter to *intermolecularly* connect the tips of two separate cofacial tetratopic ligands *via* eight heteroleptic Pt(N,O) corners[30,32,35,36] instead of *intramolecularly* bridging two adjacent tips of the same tetratopic ligand. If a ditopic linker *intramolecularly* bridges two adjacent binding sites of the tetratopic ligand *via* shared Pt(N,O) corners, then entropically more favored 1 : 2 : 4 bow-tie (⋈) complexes featuring one tetratopic core and two ditopic linkers connected by four heteroleptic corners would be formed instead of 2 : 4 : 8 tetragonal prisms containing two cofacial tetratopic faces connected by four ditopic linkers *via* eight heteroleptic corners.[54] Nevertheless, previous reports have claimed[30,33,34] that Pt(II)-driven tricomponent self-assembly of tetrapyridyl porphyrin (M′TPP, M′ = Zn- or H_2) and various aromatic and aliphatic dicarboxylate (XDC) linkers having varied lengths and rigidities yielded tetragonal prisms $[\{cis\text{-}(Et_3P)_2Pt\}_8(M'TPP)_2(XDC)_4]^{8+}$ featuring two parallel M′TTP faces and four XDC pillars connected by eight heteroligated $Pt^{II}(N,O)$ corners. The resulting complexes preserved the photophysical properties of M′TPP chromophores[33] and displayed promising applications in cancer photodynamic therapy[39] and guest encapsulation.[55] Encouraged by these literature reports,[30,33,34,39,56] we attempted to construct bi-chromophoric tetragonal prisms consisting of two M′TPP faces and four dicarboxylate linkers having complementary redox- and optically active aromatic cores, such as naphthalene- and perylene diimides that could support ligand-to-ligand photoinduced electron and/or energy transfer events. Surprisingly, none of our attempts to construct tetragonal prisms having two parallel M′TPP faces and four XDC linkers based on the reported protocols was successful despite the fact that the lengths of our XDC linkers were much longer than the distances between the two adjacent pyridyl-N atoms of free M′TPP ligands ($d_{N\text{–}N/free}$ = 10.9 Å), which precluded the possibility of intramolecular bridging of two adjacent pyridyl groups *via* heteroligated $Pt^{II}(N,O)$ corners.

Prompted by these unexpected outcomes, we took a closer look at the reported ^1H NMR spectra of the putative M′TPP-based tetragonal prisms[30,33,34,56] and recognized that all of them actually displayed two distinct singlets (1 : 1 ratio) for pyrrole protons—one set of four pyrrole protons was significantly more shielded than the other four (in contrast, all eight pyrrole protons of free M′TPP ligands are chemically equivalent and show one singlet). These NMR signatures revealed that the pyrrole rings of M′TPP ligands in these complexes were no longer chemically equivalent, *i.e.*, they resided in two completely different environments. However, in the proposed tetragonal prisms, all pyrrole rings of M′TPP should have enjoyed the same chemical environment and displayed a characteristic singlet peak.[47–49,53,55] Thus, the reported ^1H NMR signals were not consistent with the proposed tetragonal prism structures and indicated the formation of 2D bow-tie (⋈) structures, a possibility that was previously overlooked. In bow-tie (⋈) complexes, the two opposite pyrrole rings of M′TPP would be located inside two isosceles triangles formed by two parallel XDC linkers and therefore shielded accordingly, while the other two opposite pyrrole rings would remain exposed and not shielded by the XDC linkers. These inconsistencies prompted us to carefully examine whether or not the Pt(II)-driven self-assembly processes of M′TPP and XDC ligands indeed produce tricomponent prisms or yield an entirely different architecture, namely bow-ties having the same ratio (4 : 1 : 2) of the three components.

Herein, we report the self-assembly and in-depth characterization of eight novel bow-tie complexes $[\{cis\text{-}(Et_3P)_2Pt\}_4(M'TPP)(XDC)_2]\cdot 4(TfO)$ (Scheme 1) composed of M′TPP ligands (M′ = Zn and H_2) and four XDC linkers, namely 1,6-hexane-,

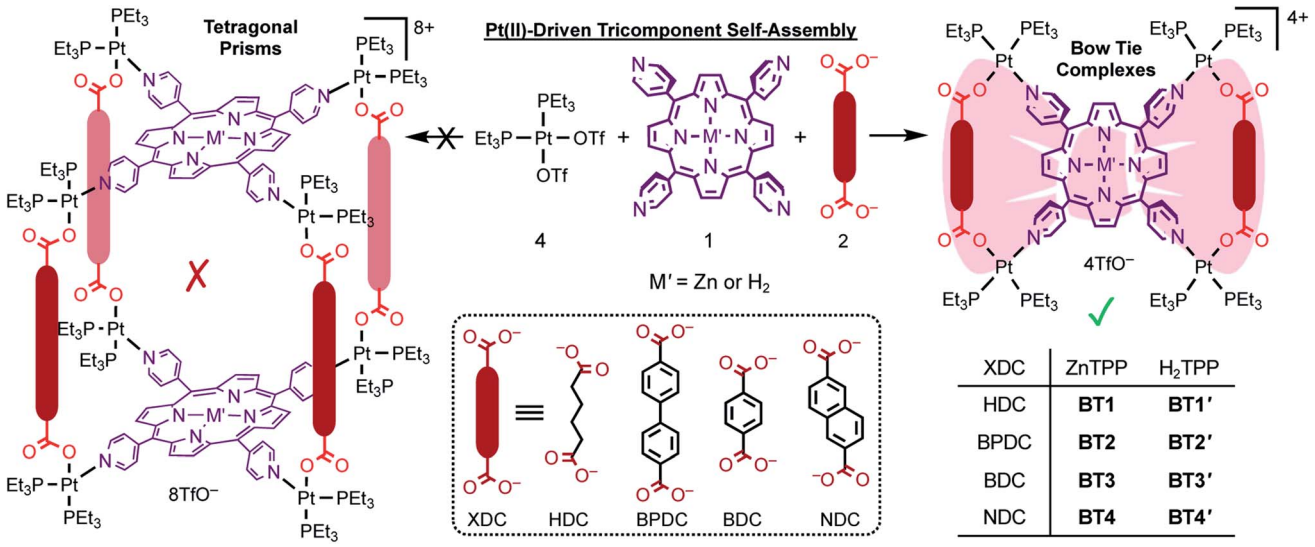

XDC	ZnTPP	H_2TPP
HDC	**BT1**	**BT1′**
BPDC	**BT2**	**BT2′**
BDC	**BT3**	**BT3′**
NDC	**BT4**	**BT4′**

Scheme 1 Pt(II)-driven self-assembly of M′TPP ligands (M′ = Zn or H_2) and four different XDC linkers (HDC, BPDC, BDC, and NDC) yielded novel bow-tie complexes $[\{cis\text{-}(Et_3P)_2Pt\}_4(M'TPP)(XDC)_2]\cdot 4(TfO)$ (**BT1**–**BT4** and **BT1′**–**BT4′**). No tetragonal prism was formed irrespective of the length and rigidity of the XDC linkers.

4,4′-biphenyl-, 1,4-benzene-, and 2,6-naphthalene- dicarboxylates (HDC, BPDC, BDC, and NDC), having different lengths and rigidities. The most direct and compelling evidence of bow-tie architectures of M′TPP-based tricomponent SCCs came from their first ever single-crystal X-ray structures, which were fully consistent with their solution phase ^{1}H, ^{31}P, and 2D (COSY, ROESY, and DOSY) NMR spectra as well as the ESI-MS data. The energy-minimized structures of these complexes were also in good agreement with the experimental results. These mutually corroborating results unequivocally demonstrated that each complex was composed of an M′TPP core and two parallel XDC linkers connected by four heteroligated $(Et_3P)_2Pt^{II}$(N,O) corners. Interestingly, the formation of M′TPP-based tricomponent bow-tie complexes instead of 3D prisms is also consistent with recent reports[54,57–59] describing the formation of similar 'triangular dicycles' based on other tetratopic cores and ditopic linkers. Furthermore, we demonstrate the ability of an electron rich ZnTPP-based bow-tie complex to form a π-donor/acceptor (D/A) charge-transfer (CT) complex with highly electron deficient 1,4,5,8,9,12-hexaazatriphenylene-2,3,6,7,10,11-heaxacarbonitrile (HATHCN) but not with another π-donor such as pyrene.

Results and discussion

Heteroleptic coordination-driven self-assembly of M′TPP-based tricomponent bow-ties (⋈)

To determine whether the heteroleptic coordination of *cis*-$(Et_3P)_2Pt^{II}$ corners with tetratopic M′TPP ligands and ditopic XDC linkers yield tetragonal 3D prisms containing two cofacial M′TPP ligands and four XDC linkers held together by eight Pt(II) corners[30,33,34] or 2D bow-ties containing a M′TPP core and two parallel XDC linkers connected by four shared Pt(II) corners, herein, we employed four XDC ligands—HDC, BPDC, BDC, and NDC—having different lengths, rigidities, and electron densities. For consistency, we applied the same self-assembly conditions reported in the literature,[30,33,34] namely (i) 4 : 1 : 2 stoichiometry of *cis*-$(Et_3P)_2Pt(TfO)$, M′TPP, and XDC; (ii) solvent mixtures (1 : 1 : 1 CH_2Cl_2/MeCN/$MeNO_2$ or 4 : 1 Me_2CO/H_2O) that adequately solubilized all components; (iii) temperature (~60 °C), and (iv) reaction time (~18 h) that were used to synthesize the proposed prisms. Our comprehensive 1D and 2D NMR, ESI-MS, single-crystal X-ray, and computational studies unequivocally demonstrated that regardless of their rigidity and lengths (~7–11 Å), all four XDC linkers formed bow-tie complexes **BT1–BT4** and **BT1′–BT4′** (Scheme 1, Fig. 1) while no 3D prism was identified. Notably, the HDC and BDC linkers were also previously employed to assemble M′TPP-based tricomponent SCCs,[30,33,34,39] and the reported NMR spectra of the resulting complexes were the same as those of our unequivocally characterized bow-tie structures.

Single-crystal structures of bow-tie complexes

The single-crystal X-ray analysis of these tricomponent SCCs presented the most direct and conclusive evidence of their bow-tie structures consisting of a M′TPP core and two parallel XDC linkers held together by four heteroleptic $(Et_3P)_2Pt$(N,O) corners

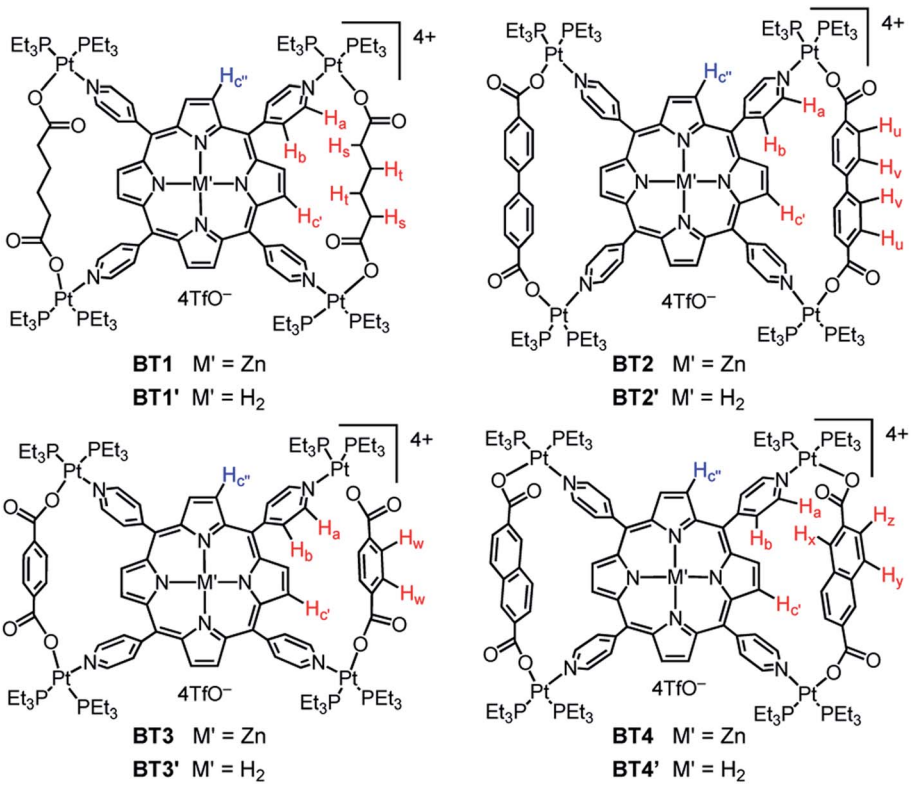

Fig. 1 The chemical structures of bow-tie complexes.

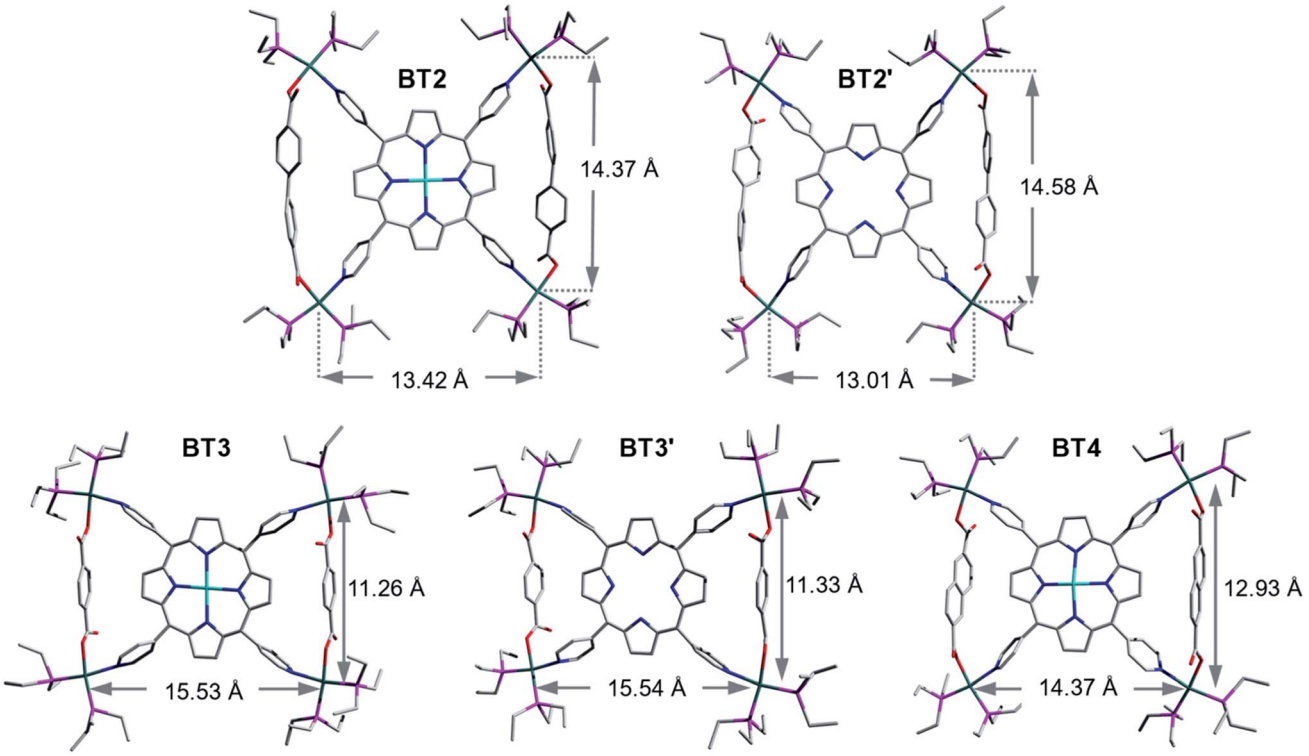

Fig. 2 Single-crystal structures of **BT2**, **BT2′**, **BT3**, **BT3′** and **BT4** bow-tie complexes. Atom legends: green: Pt, cyan: Zn, pink: P, red: O, blue: N, and grey: C. The H-atoms and TfO^- anions were omitted for clarity.

(Fig. 2). Notably, this was the first time the crystal structures of any M′TPP-based tricomponent SCCs could be determined. The crystals were obtained from the respective NMR solutions (acetone-d_6) *via* either slow evaporation or vapor diffusion of CH_2Cl_2 or Et_2O, assuring that the solid-state crystal structures and solution NMR data belonged to the same materials. The bow-tie complexes based on rigid aromatic BPDC, BDC, and NDC linkers crystallized easily, but those containing flexible aliphatic HDC linkers did not. The structural features of all bow-tie complexes (Table 1) were fully consistent with their respective NMR and ESI-MS data, confirming that the same species were present both in solutions and solid crystals. The crystal structures of these bow-tie complexes shined light on why the M′TPP core displayed two distinct ^{1}H NMR signals for the enclosed $H_{c'}$ and exposed $H_{c''}$ protons (Fig. 1) and why only $H_{c'}$ protons were shielded by and ROE-coupled to XDC linkers but $H_{c''}$ protons were not.

The bow-tie (⋈)-shaped **BT2** and **BT2′** complexes (Fig. 2: $[\{(Et_3P)_2Pt\}_4(M'TPP)(BPDC)_2]^{4+}$, M′ = Zn or H_2) crystallized in the $P\bar{1}$ and $C2/c$ space groups, respectively. The ∠N–Pt–O angles of slightly distorted square-planar Pt(II) corners ranged between *ca.* 82–85° (two diagonally opposite angles were the same). In

Table 1 Key structural parameters of bow-tie complexes obtained from their single-crystal structures. The parameters obtained from the calculated structures are labeled with asterisks (*)

	BT1 calc.*	**BT2**	**BT2′**	**BT3** (calc.*)	**BT3′** (calc.*)	**BT4**
Space group	—	$P\bar{1}$	$C2/c$	$C2/c$	$I4_1/a$	$P2_1/c$
$d_{Pt-Pt/int}$ (Å)	11.55*	14.37	14.58	11.26 (11.33*)	11.33 (11.33*)	12.93
$d_{Pt-Pt/ext}$ (Å)	15.41*	13.42	13.01	15.53 (15.59*)	15.54 (15.56*)	14.37
$d_{N-N/int}$ (Å)	10.19*	11.38	11.52	10.09 (10.12*)	10.07 (10.20*)	10.83
$d_{N-N/ext}$ (Å)	11.63*	10.37	10.18	11.39 (11.69*)	11.61 (11.68*)	10.80
$d_{Hc'-XDC-center}$ (Å)	2.84*	3.37	3.11	3.18 (3.50*)	3.05 (3.44*)	2.95
$d_{Hc'-pyridine-center}$ (Å)	2.96*	3.41	3.51	3.02 (2.98*)	2.96 (3.01*)	3.19
$d_{Hc''-pyridine-center}$ (Å)	3.37*	3.08	3.00	3.41 (3.47*)	3.47 (3.41*)	3.26
∠N–Pt–O (°)	96*, 98*	82, 85	82, 83	78, 83 (93*)	80, 83 (93*)	82, 82
$\angle(N_{Py}-center-N_{Py})_{int}$ (°)	82*	95	97	83 (81*)	82 (82*)	88
$\angle(N_{Py}-center-N_{Py})_{ext}$ (°)	98*	85	83	97 (99*)	98 (98*)	89
$\theta_{porphyrin/pyridyl-dh}$ (°)	82*, 83*	76, 77	64, 73	86, 88 (84*)	76, 80 (85*)	65, 76
$\theta_{pyrrole/XDC-dh}$ (°)	—	—	—	80 (90*)	85 (90*)	87

BT2 and **BT2′**, the distances between two BPDC-bridged Pt(II) corners ($d_{Pt-Pt/int}$) were *ca.* 14.5 and 14.6 Å, respectively, whereas those between two adjacent Pt(II) corners not bridged by BPDC ($d_{Pt-Pt/ext}$) were 13.4 and 13.0 Å, respectively. This happened because the long BPDC linker (l_{BPDC} = 11.2 Å)[60] positioned the two bridged Pt(II) corners farther away from each other, which in turn shortened the $d_{Pt-Pt/ext}$. Consequently, the distances between the two adjacent pyridyl-N atoms coordinated to two BPDC-bridged Pt(II) corners, *i.e.*, the pyridyl-N atoms that belonged to the same isosceles triangle, were also noticeably longer ($d_{N-N/int} \approx$ 11.4 and Å) than the distance between two adjacent pyridyl-N atoms that were not part of the same triangle ($d_{N-N/ext} \approx$ 10.4 Å). These N–N distances in **BT2** and **BT2′** deviated from the uniform distance between two adjacent pyridyl-N atoms of free M′TPP ligands ($d_{N-N/free} \approx$ 10.9 Å).[61,62] Furthermore, in **BT2**, the angles of projection between two adjacent pyridyl rings that belonged to the same triangle ($\angle(N_{Py}\text{–center–}N_{Py})_{int}$) expanded to 95° (97° in **BT2′**), while the angle between two adjacent pyridyl rings that were not part of the same triangle ($\angle(N_{Py}\text{–center–}N_{Py})_{ext}$) contracted to 85° (83° in **BT2′**). Thus, these angles deviated by 3–5° from the angles of projection (~90°) between the adjacent pyridyl rings of free M′TPP in order to incorporate long BPDC linkers within the isosceles triangles of bow-tie structures. The dihedral angles between the porphyrin core and the pyridyl arms were 76° in **BT2** (73° in **BT2′**). The enclosed pyrrole rings of M′TPP and the twisted BPDC core (torsion angle between two phenyl rings ≈ 40°) located across the bay were not coplanar but formed large dihedral angles. The average distances from the enclosed $H_{c'}$ pyrrole protons located inside the triangles to the center of the closest phenyl ring of the BPDC linker ($d_{Hc'-XDC}$) was *ca.* 3.4 Å in **BT2** (3.1 Å in **BT2′**) and to the center of the nearest pyridyl ring ($d_{Hc'-pyridine-center}$) was 3.4 Å in **BT2** (3.5 Å in **BT2′**). Both distances were the longest among the bow-tie complexes presented here.

Although the entire single-crystal structures of **BT2** and **BT2′** complexes, including their ancillary Et_3P ligands on the Pt(II) corners, were well-resolved, only the basic bow-tie skeletons of **BT3**, **BT3′**, and **BT4** complexes consisting of the M′TPP core, two parallel BDC and NDC linkers, and four Pt(II) corners were fully resolved, but the fluxional CH_3CH_2-groups and TfO^- anions were not, which caused large *R*-values. Nevertheless, since the ancillary ligands and counterions were not integral parts of the bow-tie structures, the poor resolution of these highly disordered components had little effect on key structural features that influenced their respective NMR spectra.

The BDC-based bow-tie complexes **BT3** and **BT3′** (Fig. 2: $[\{(Et_3P)_2Pt\}_4(M'TPP)(BDC)_2]^{4+}$, M′ = Zn or H_2) crystallized in *C*2/*c* and $I4_1/a$ space groups, respectively. The ∠N–Pt–O angles at distorted square-planar Pt(II) corners ranged between *ca.* 78–83°. The distances between two adjacent Pt(II) corners bridged by short BDC linkers (l_{BDC} = 6.9 Å)[60] were *ca.* 11.3 Å ($d_{Pt-Pt/int}$), whereas the distances between two adjacent Pt(II) corners not bridged by BDC ($d_{Pt-Pt/ext}$) were *ca.* 15.5 Å. Thus, the short BDC linkers placed the two bridged Pt(II) corners closer to each other while increasing the distances between the two non-bridged Pt(II) corners. Consequently, the distances between the pyridyl-N atoms that belonged to the same triangle were also shorter ($d_{N-N/int} \approx$ 10.1 Å) than those between two pyridyl-N atoms that were not part of the same triangle ($d_{N-N/ext} \approx$ 11.5 Å). Consequently, the projection angles between two adjacent pyridyl rings belonging to the same triangle ($\angle(N_{Py}\text{–center–}N_{Py})_{int}$) shrunk to *ca.* 82°, while the angles between two adjacent pyridyl rings not belonging to the same triangle ($\angle(N_{Py}\text{–center–}N_{Py})_{ext}$) expanded to *ca.* 98° (*ca.* 8° deviations from the ideal ~90° angle in free M′TPP) in order to accommodate short BDC linkers within the triangles. The dihedral angles between the enclosed pyrrole rings of M′TPP and the BDC core located across the bay were 80–85°, *i.e.*, they were almost orthogonal to each other. The enclosed $H_{c'}$ pyrrole protons were projected toward the center of the BDC ring ($d_{Hc'-XDC} \approx$ 3.1 Å) and the adjacent pyridyl rings, which were pulled closer ($d_{Hc'-pyridine-center} \approx$ 3 Å) by the BDC linker.

The NDC-based bow-tie complex **BT4** $[\{(Et_3P)_2Pt\}_4(ZnTPP)(NDC)_2]^{4+}$ (Fig. 2) possessed the $P2_1/c$ space group. All four ∠N–Pt–O angles of distorted square-planar Pt(II) corners were *ca.* 82°. The distances between two adjacent NDC-bridged Pt(II) corners ($d_{Pt-Pt/int}$ = 12.9 Å) were slightly shorter than those between two adjacent Pt(II) corners not bridged by a NDC linker ($d_{Pt-Pt/ext}$ = 14.4 Å). However, the distances between the N-atoms of two adjacent pyridyl rings belonging to the same triangle ($d_{N-N/int}$) and those between two adjacent pyridyl-N atoms that were not part of the same triangle ($d_{N-N/ext}$) were almost same (*ca.* 10.8 Å) and close to the uniform distances between two adjacent pyridyl-N atoms of the free ZnTPP ligand ($d_{N-N/free}$ ~ 10.9 Å). As a result, the angles between two adjacent pyridyl rings belonging to the same triangle ($\angle(N_{Py}\text{–center–}N_{Py})_{int}$) and those between two adjacent pyridyl rings not belonging to the same triangle ($\angle(N_{Py}\text{–center–}N_{Py})_{ext}$) in **BT4** were also close to ideal ~90° angle between adjacent pyridyl rings found in the free ZnTPP ligand. Thus, the intermediate length of the NDC linker (l_{NDC} = 9.2 Å)[60] caused the least distortion of the ZnTPP ligand in order to form the isosceles triangles. In **BT4**, the ZnTPP and the NDC planes were nearly orthogonal to each other (dihedral angles = 87°). The enclosed $H_{c'}$ pyrrole protons located inside the triangles were projected toward the NDC core across the bay ($d_{Hc'-XDC} \approx$ 3 Å) and to the center of the adjacent pyridyl rings ($d_{Hc'-pyridine-center} \approx$ 3.2 Å).

Energy optimized structures

Since the crystal structures of **BT1** or **BT1′** complexes containing flexible HDC linker were not available, we calculated their energy minimized structures using Gaussian 09 software (Fig. 3). To verify the accuracy of these calculated structures, we also calculated the energy minimized structures of BDC-based bow-tie complexes, which were in good agreement with their actual crystal structures (Table 1). In **BT1** and **BT1′** complexes, the ∠N–Pt–O angles at the distorted square-planar Pt(II) corners were *ca.* 96–98°. The two adjacent HDC-bridged Pt(II) corners ($d_{Pt-Pt/int}$) were located *ca.* 11.6 Å apart, whereas the two adjacent Pt(II) corners not bridged by HDC ($d_{Pt-Pt/ext}$) were located *ca.* 15.4 Å apart. The bridged Pt–Pt distances in **BT1** were comparable to those found in **BT3**, suggesting that HDC and BDC have similar

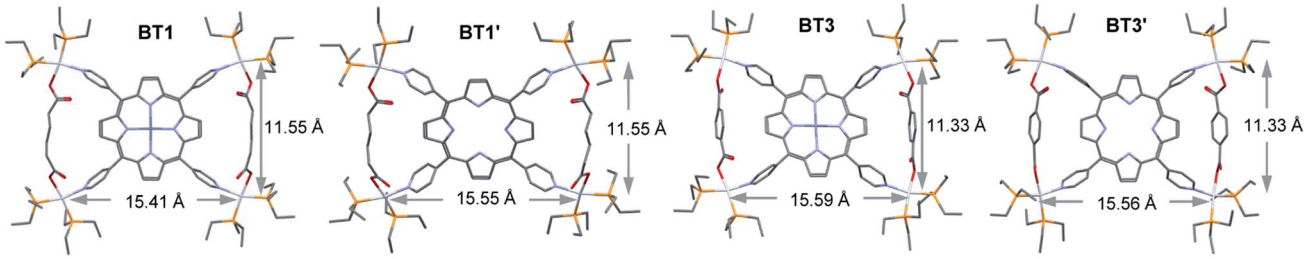

Fig. 3 The optimized structures of **BT1**, **BT1′**, **BT3**, and **BT3′** complexes calculated by the PM6 method.

lengths. Like BDC, the short HDC linkers also brought the two bridged Pt(II) corners closer to each other, expanding the distances between the two adjacent non-bridged Pt(II) corners. Consequently, the angles between two adjacent pyridyl rings of M′TPP that belonged to the same triangle ($\angle(N_{Py}\text{–center–}N_{Py})_{int}$) shrunk to ~82°, while the angles between the two adjacent pyridyl rings that were not part of the same triangle ($\angle(N_{Py}\text{–center–}N_{Py})_{ext}$) expanded to ~98° in order to accommodate short HDC linkers within the isosceles triangles of these bow-tie structures. The distances from the enclosed $H_{c'}$ pyrrole protons to the center of the nearest pyridyl ring ($d_{Hc'\text{–pyridine-center}}$) were *ca.* 2.96 Å and to the H_t protons of the HDC linker located across the bay were *ca.* 2.8 Å. The calculated structures of these complexes were consistent with their respective NMR spectra.

Thus, the single-crystal and energy-minimized structures of M′TPP-based tricomponent SCCs demonstrated that regardless of the length (within the range of 6.9–11.2 Å) and rigidity of the XDC linkers, the Pt(II)-driven self-assembly of M′TPP and XDC ligands yielded bow-tie complexes instead of 3D prisms. This happened because the pyridyl arms of M′TPP ligands deviated from their original projections in order to incorporate the XDC linkers within the isosceles triangles of bow-tie structures.

^{31}P NMR spectroscopy

Simultaneous coordination of a pyridyl group of M′TPP and a carboxylate group of XDC with *cis*-$(Et_3P)_2Pt^{II}$ was also evident from the ^{31}P NMR spectra of the resulting SCCs (Fig. 4 and S1†).

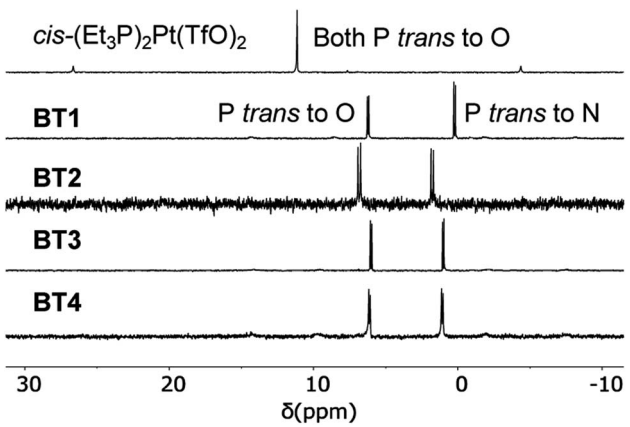

Fig. 4 Partial ^{31}P NMR spectra (122 MHz, acetone-d_6) of the *cis*-$(Et_3P)_2Pt(TfO)_2$ and **BT1**–**BT4** complexes.

While *cis*-$(Et_3P)_2Pt(TfO)_2$ displayed a characteristic singlet at 11.14 ppm indicating that both Pt(II)-coordinated P atoms were chemically equivalent, the resulting **BT1**–**BT4** and **BT1′**–**BT4′** complexes displayed two distinct doublets—one at *ca.* 0–2 ppm that corresponded to the P-nucleus *trans*- to the pyridyl-N atom and another at 6–7 ppm ($^2J_{P\text{–}P} \approx$ 20–21 Hz) corresponding to the P-nucleus *trans*- to the carboxylate O-atom—indicating that the two ancillary Et_3P ligands were not chemically equivalent.[30,33,34] The fact that no other ^{31}P NMR signal was observed further confirmed the exclusively heteroleptic coordination of two different ligands with the Pt(II) corners and ruled out the formation of any homoleptic complex. However, the ^{31}P NMR spectra shed little light on the actual structures and compositions of the resulting tricomponent SCCs, *i.e.*, whether they were 3D prisms or 2D bow-ties, as both structures would feature the same heteroleptic *cis*-$(Et_3P)_2Pt^{II}(N,O)$ corners.

^{1}H NMR spectroscopy

The ^{1}H NMR spectra of the resulting complexes (Fig. 5, S2 and S3†) also presented telltale signs of their bow-tie structures and ruled out tetragonal prism formation. In comparison to the D_{4h}-symmetric free ZnTPP ligand, which displayed two doublets at 8.58 and 7.95 ppm corresponding to its H_a and H_b pyridyl protons (8 each), respectively, and a sharp singlet at 8.61 ppm for all eight chemically equivalent H_c pyrrole protons (Fig. 5), the **BT1**–**BT4** complexes not only displayed a significant down-field shift of H_a and H_b pyridyl protons due to Pt(II)-coordination, but most tellingly, two distinct singlets with a 1 : 1 integral ratio for $H_{c'}$ and $H_{c''}$ (pyrrole) protons indicating that the pyrrole rings of ZnTPP were no longer chemically equivalent. The H_2TPP-based **BT1′**–**BT4′** complexes (Fig. S2†), and all previously reported M′TPP-based tricomponent SCCs,[30,33,34] also displayed two distinct singlets for the pyrrole protons, which indicated that the pyrrole rings of M′TPP resided in two different environments, a telltale sign of bow-tie complexes, not prisms.

The singlet peaks corresponding to four $H_{c'}$ pyrrole protons of the **BT1**–**BT4** complexes appeared at 8.38, 7.73, 7.13, and 6.79 ppm, respectively, which were significantly up-field shifted from the H_c signal (8.61 ppm) of free ZnTPP, while the singlets corresponding to four $H_{c''}$ pyrrole protons appeared at 9.18, 8.52, 9.16, and 8.86 ppm, respectively. Thus, the up-field shifts of $H_{c'}$ signals were directly correlated to the increasing electron cloud, *i.e.*, the shielding effect of XDC linkers (HDC < BPDC < BDC < NDC), suggesting that these pyrrole protons were located

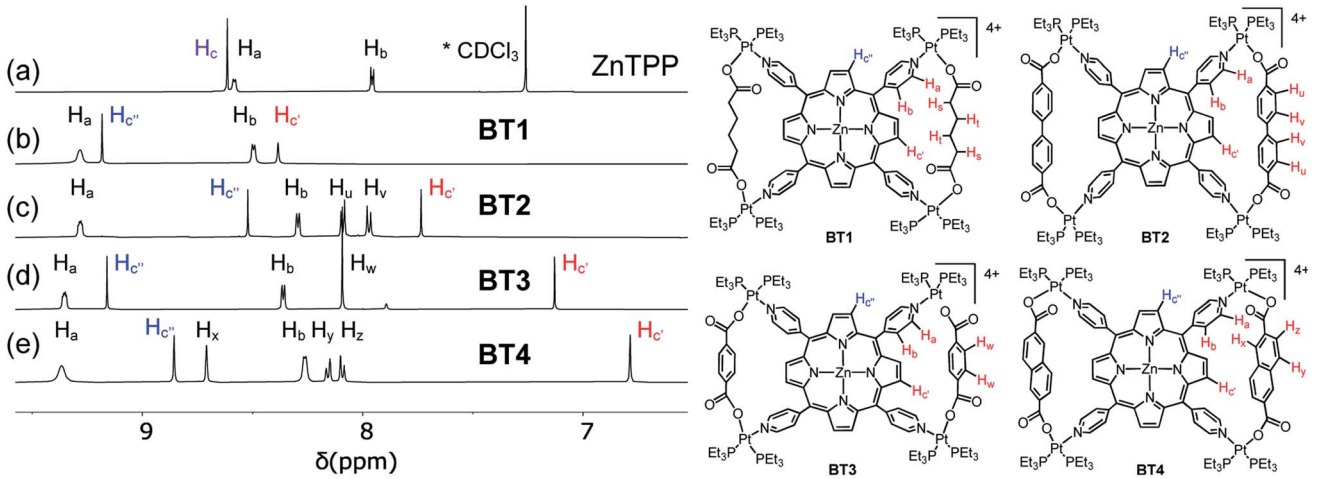

Fig. 5 Partial ^{1}H NMR spectra (500 MHz) of (a) ZnTPP, (b) **BT1**, (c) **BT2**, (d) **BT3**, and (e) **BT4**. The enclosed $H_{c'}$ pyrrole protons (highlighted in red) located inside the isosceles triangles of bow-tie structures were shielded by adjacent XDC linkers, whereas the exposed $H_{c''}$ pyrrole protons (highlighted in blue) were not.

inside the isosceles triangles formed by two parallel XDC linkers, whereas the $H_{c''}$ pyrrole protons were not. The aliphatic HDC linkers in **BT1** exerted the least shielding effect, causing the smallest up-field shift of the enclosed $H_{c'}$ pyrrole protons located across the bay, followed by the BPDC linkers having two twisted phenyl rings that were not properly aligned with the enclosed $H_{c'}$ pyrrole protons of **BT2**, as seen from its single-crystal structure (*vide supra*). Having the largest π-cloud and the maximum shielding effect among the four XDC linkers employed here, the NDC linkers in **BT4** caused the largest up-field shift of enclosed $H_{c'}$ protons, followed by the BDC linkers in **BT3**. Although the exposed $H_{c''}$ pyrrole protons were not shielded by distant XDC linkers, their chemical shifts were affected by the length of the XDC linkers, which controlled their distances from the adjacent pyridyl rings of ZnTPP. This was further evident from their crystal structures and certain structural features summarized in Table 1. For instance, the shorter HDC and BDC linkers ($l \approx 7$ Å) placed the bridged Pt(II) corners closer to each other, which in turn, pulled the pyridyl rings of the ZnTPP ligand away from the exposed $H_{c''}$ pyrrole protons of the **BT1** and **BT3** complexes. As a result, the shielding effect of pyridyl rings on $H_{c''}$ pyrrole protons in **BT1** and **BT3** was diminished, and they appeared at more downfield positions (*ca.* 9.2 ppm) than the H_c protons of the free ZnTPP ligand. On the other hand, the longest BPDC linkers ($l_{BPDC} = 11.2$ Å) in **BT2** held the bridged Pt(II) corners farther away from each other, which in turn, pushed the pyridyl rings of ZnTPP closer to the exposed $H_{c''}$ pyrrole protons making them more shielded and up-field shifted than the H_c protons of free ZnTPP. Having an intermediate length, the NDC linkers ($l_{NDC} = 9.2$ Å) in **BT4** pulled the pyridyl rings of ZnTPP slightly away from exposed $H_{c''}$ protons, causing a slight downfield shift. The exact same trends were observed for H_2TPP-based **BT1′**–**BT4′** complexes (Fig. S2†).

Thus, the splitting of pyrrole protons of M′TPP ligands into two chemically nonequivalent and noncoupled $H_{c'}$ and $H_{c''}$ protons in the tricomponent SCCs and the variable shielding of the former by XDC linkers were the unmistakable signs of bow-tie complexes where two opposite pyrrole rings bearing four $H_{c'}$ protons were located inside the isosceles triangles formed by two parallel XDC linkers while the other two pyrrole rings bearing four $H_{c''}$ protons remained exposed. It is worth noting that previously reported M′TPP-based tricomponent SCCs, including those containing HDC and BDC ligands,[32,33] essentially displayed the same ^{1}H NMR characteristics as those displayed by our **BT1**–**BT4** and **BT1′**–**BT4′** complexes, *i.e.*, two distinct singlets for $H_{c'}$ and $H_{c''}$ pyrrole protons, which are the characteristic signs of bow-tie structures. If the resulting tricomponent SCCs were indeed tetragonal prisms having two cofacial M′TPP planes connected by four XDC linkers *via* heteroleptic $(Et_3P)_2Pt^{II}(N,O)$ corners,[30,33,34,56] then all sixteen pyrrole protons of M′TPP faces should have remained chemically equivalent and displayed one singlet peak instead of splitting into two chemically non-equivalent $H_{c'}$ and $H_{c''}$ protons with two distinct singlets, as observed in other porphyrin-based prisms.[47–49,53,55] However, that was not observed for any Pt(II)/M′TPP/XDC-based tricomponent SCCs,[30,33,34,56] which ruled out the prism formation.

^{1}H–^{1}H COSY NMR spectroscopy

The COSY NMR spectra of these M′TTP-based tricomponent SCCs (Fig. S4†) provided further insights into their actual structures by revealing the coupling between the adjacent (α- and β-) protons. Conspicuously missing from the COSY NMR spectra of all these SCCs were any α/β-coupling between the $H_{c'}$ and $H_{c''}$ protons of the M′TPP ligand, which further indicated that these two chemically non-equivalent protons did not belong to the same pyrrole ring but to two separate pyrrole rings located in different environments. This scenario was possible only in bow-tie structures where two opposite pyrrole rings carrying the $H_{c'}$ protons were located inside the triangles, whereas the other two pyrrole rings bearing $H_{c''}$ protons remained exposed. If these tricomponent SCCs were indeed

tetragonal prisms containing two cofacial M′TPP panels linked by four XDC linkers, then either all the pyrrole protons of M′TPP should have remained chemically equivalent instead of splitting into distinct $H_{c'}$ and $H_{c''}$ protons, or each pyrrole ring would have carried one $H_{c'}$ and one $H_{c''}$ protons involved in α/β-coupling (in case of twisted prisms).[63] The absence of such couplings ruled out the prism formation.

ROESY NMR spectroscopy

Another piece of powerful evidence of bow-tie complex formation was found in the ROESY NMR spectra (Fig. 6 and S5†), which revealed long-range coupling between the enclosed $H_{c'}$ pyrrole protons of M′TPP and the XDC protons located across the bay. For example, the enclosed $H_{c'}$ pyrrole protons were coupled with (i) the H_t protons of HDC in **BT1** and **BT1′**, (ii) the H_u and H_v protons of BPDC in **BT2** and **BT2′**, (iii) the H_w protons of BDC in **BT3** and **BT3′**, and (iv) the H_x, H_y, and H_z protons of NDC in **BT4** and **BT4′**, indicating that the enclosed pyrrole rings were located in close proximity to the XDC linkers. In addition, the enclosed $H_{c'}$ protons were also coupled to the adjacent H_b pyridyl protons of M′TPP ligands. However, no such ROE-coupling between the exposed $H_{c''}$ pyrrole protons and the distant XDC protons were observed (the $H_{c''}$ protons were only coupled to H_b protons of the adjacent pyridyl ring in some cases), further verifying that the enclosed $H_{c'}$ and exposed $H_{c''}$ pyrrole protons were located in two different chemical environments. This scenario is possible only in bow-tie structures, not in prisms.

DOSY NMR spectroscopy

Diffusion NMR experiments (acetone-d_6) showed that (Fig. S6†) irrespective of the length of XDC linkers ($l \approx 7$–11 Å), the **BT2**, **BT3**, and **BT4** complexes possessed similar diffusion coefficients ($D = 5.40 \times 10^{-10}$, 5.63×10^{-10}, and 5.67×10^{-10} m^2 s^{-1}, respectively) and hydrodynamic radii (r_H = 12.64, 12.11, and 12.04 Å, respectively). Notably, the hydrodynamic radii of these complexes were roughly two-third of a legitimate porphyrin-based tetragonal prism (r_H = 17.54 Å),[47] and they were not affected by the length of XDC linkers (the longer linkers should have yielded larger cages but did not affect the overall size of 2D

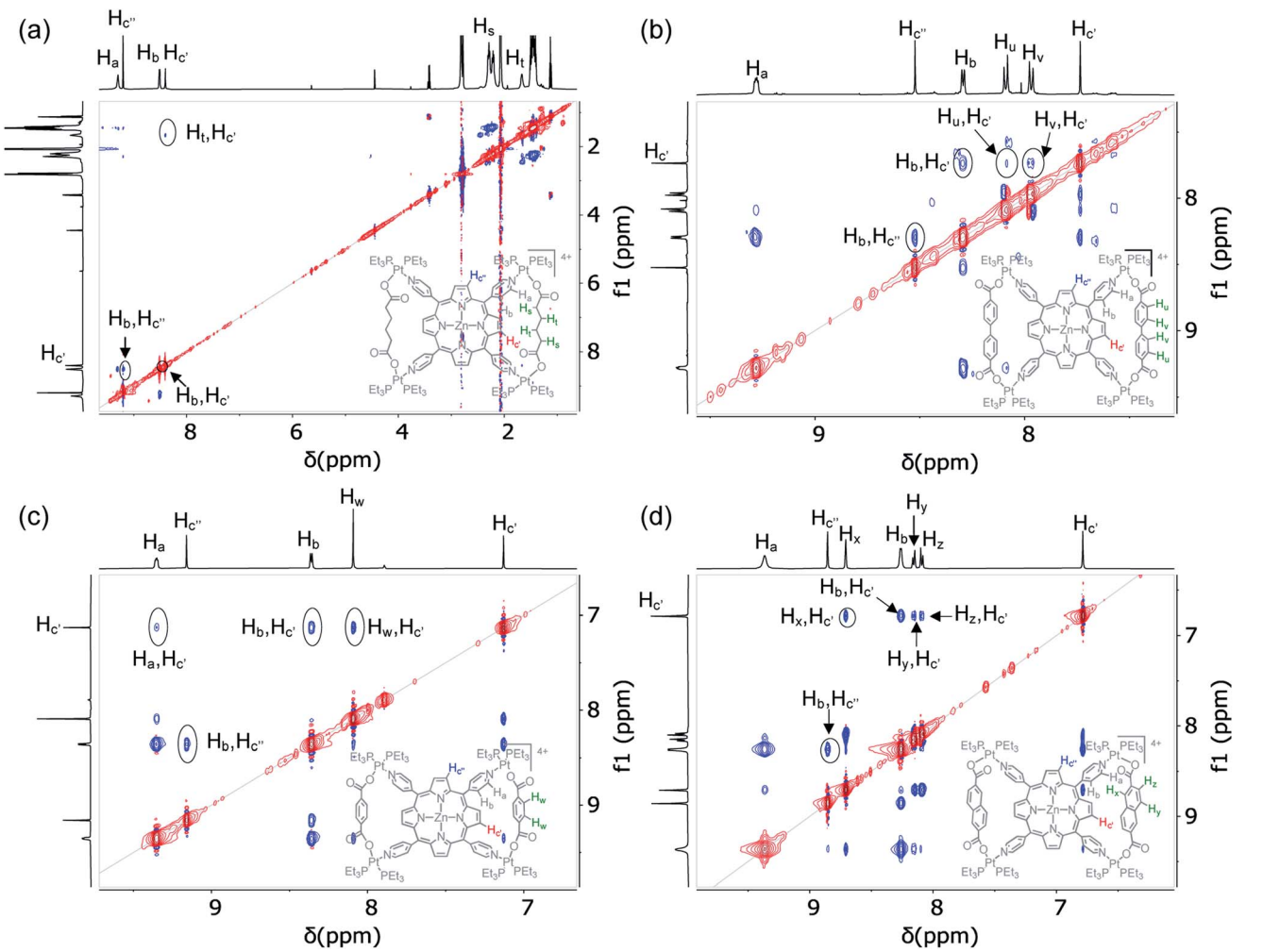

Fig. 6 Partial ^{1}H–^{1}H ROESY NMR spectra (500 MHz, acetone-d_6) of (a) **BT1**, (b) **BT2**, (c) **BT3**, and (d) **BT4** show that the enclosed $H_{c'}$ pyrrole protons of these bow-tie complexes located inside the isosceles triangles are through-space coupled with the protons of adjacent XDC linkers but the exposed $H_{c''}$ pyrrole protons are not coupled with the distant XDC protons.

bow-tie complexes), which further ruled out the alleged cage formation.

ESI-MS analysis

The ESI-MS analysis revealed (Fig. S7†) the characteristic *m*/*z* peaks of the $[M\text{-}2TfO]^{2+}$ species of bow-tie complexes. The ZnTPP-based **BT1–BT4** and H_2TPP-based **BT2′**, **BT3′**, and **BT4′** displayed the respective $[M\text{-}2TfO]^{2+}$ peaks at *m*/*z* = 1497.09, 1593.58, 1517.01, 1567.05, 1561.50, 1485.52, and 1535.60, but no peak corresponding to any tetragonal prisms. Interestingly, the previously reported[30] ESI-MS profile of a tricomponent SCC featuring $(Et_3P)_2Pt^{II}$, H_2TPP, and BDC revealed a prominent *m*/*z* peak at 1481.38, which possibly represented the $[M\text{-}2PF_6^-]^{2+}$ species of the bow-tie complex $[\{(Et_3P)_2Pt\}_4(H_2TPP)(BDC)_2]^{4+}\cdot 4(PF_6^-)$. Although previous reports have assigned certain *m*/*z* peaks to $[\{(Et_3P)_2Pt\}_8(M'TPP)_2(XDC)_4]^{8+}\cdot 8(X^-)$ prisms,[30,33,34,56,64] in light of our extensive X-ray crystallographic and NMR analyses, those peaks could be attributed to dimers of $[\{(Et_3P)_2Pt\}_4(M'TPP)(XDC)_2]^{4+}\cdot 4(X^-)$ bow-tie complexes (after the loss of certain counterions) instead of any prisms. Thus, in light of the discovery of M′TPP-based tricomponent bow-tie complexes and a better understanding of why the corresponding tetragonal prisms were not formed, it appears that careful 2D NMR and X-ray crystallographic studies are vital for accurate structural characterization of similar tricomponent SCCs.

Molecular recognition *via* π-donor/acceptor charge transfer interaction

Having assembled and accurately characterized M′TPP-based novel tricomponent bow-tie complexes, we turned our attention to explore their molecular recognition capabilities. We hypothesized that the electron-rich M′TPP core of bow-tie complexes will selectively recognize electron deficient π-systems through π-donor/acceptor CT interaction but not other π-donors. To test this hypothesis, we employed **BT4** ($[\{(Et_3P)_2Pt\}_4(ZnTPP)(NDC)_2]^{4+}$) as a host, which contains the least strained ZnTPP ligand (*i.e.*, $\angle(N_{Py}\text{–}Zn\text{–}N_{Py})_{int} \approx \angle(N_{Py}\text{–}Zn\text{–}N_{Py})_{ext} \approx 88\text{–}89^\circ$) because of the intermediate length of the rigid NDC linker, and highly electron-deficient HATHCN and electron-rich pyrene compounds as potential guests.

The **BT4**·HATHCN complex formation was evident from the ^{1}H NMR titration experiment (Fig. 7a). The characteristic $H_{c'}$ and $H_{c''}$ (pyrrole) protons of the ZnTPP core gradually shifted up-field with the increasing amount of HATHCN (it has no

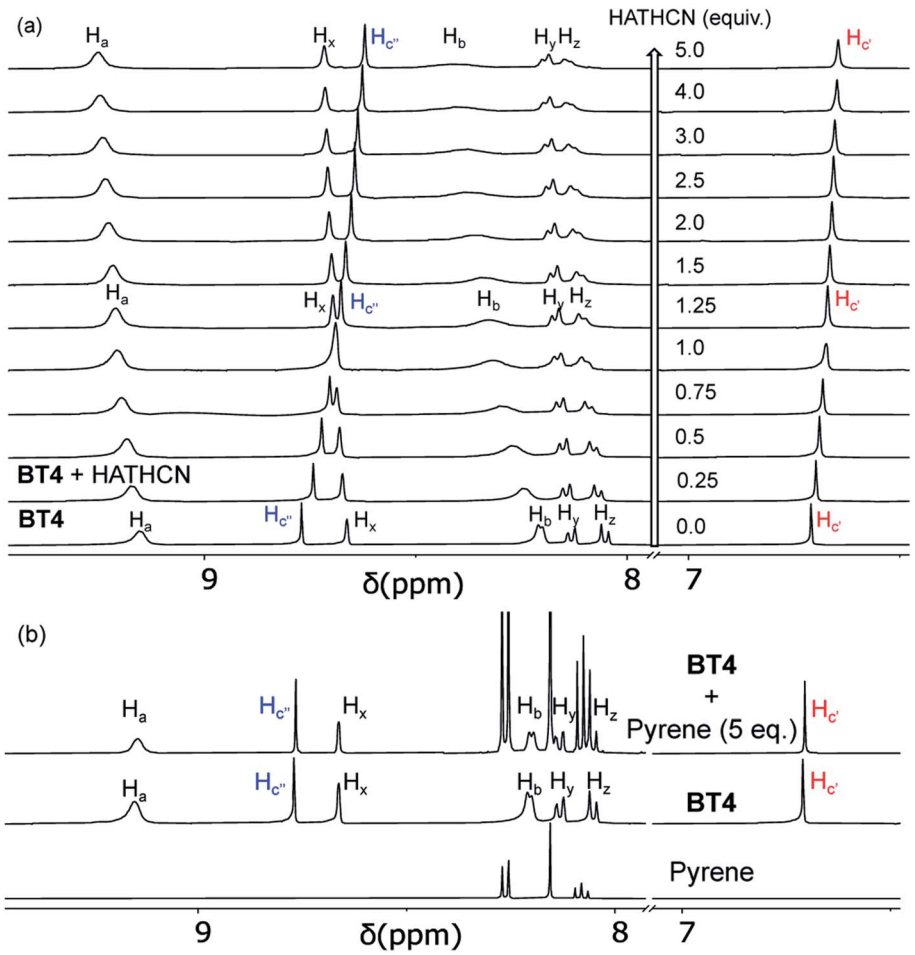

Fig. 7 The ^{1}H NMR titration data (500 MHz, 3 : 7 CD_2Cl_2/CD_3NO_2) of **BT4** with (a) HATHCN and (b) pyrene show gradual up-field shift, *i.e.*, shielding of $H_{c'}$ and $H_{c''n}$ (pyrrole) signals of the ZnTPP core by the former but no such change with the latter.

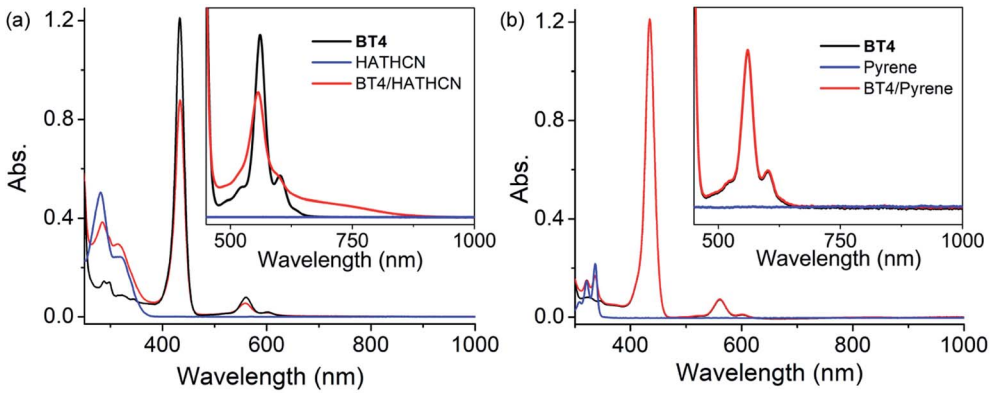

Fig. 8 The UV-vis spectra of **BT4** (in CH_2Cl_2) in the presence of (a) HATHCN and (b) pyrene. Insets: the amplified 475–1000 nm regions show the appearance of the CT band with HATHCN but not with pyrene.

proton), revealing that the ZnTPP core was shielded by cofacially aligned HATHCN. The greater up-field shift and shielding of $H_{c''}$ signal ($\Delta\delta = 0.15$ ppm) than $H_{c'}$ signal ($\Delta\delta = 0.06$ ppm) suggests that HATHCN is positioned more above the exposed pyrrole rings than sterically crowded (by NDC) enclosed pyrrole rings. The protons on the pyridyl and NDC rings, which are aligned almost perpendicularly to the Zn-porphyrin and HATHCN cores, shifted downfield, indicating that they were not shielded by HATHCN. The formation constant of the **BT4**·HATHCN complex ($K_a = 2.5 \times 10^3$ M^{-1}, 3 : 7 CD_2Cl_2/CD_3NO_2, 25 °C) calculated from the ^{1}H NMR titration data (Fig. S8†)[65] is comparable to that of similar CT complexes of other electron-rich Zn-porphyrin and π-acidic HAT-derivatives.[66] In contrast, during ^{1}H NMR titration of **BT4** with pyrene (Fig. 7b), none of their signals shifted, indicating the lack of any meaningful interaction between the two electron-rich species. The ^{31}P NMR spectrum of **BT4** remained unchanged in the presence of HATHCN (Fig. S9†), confirming that it did not interfere with the heteroleptic coordination of $(Et_3P)_2Pt^{2+}$ corners with the ZnTPP and NDC ligands. The ESI-MS analysis also revealed the $[M\text{-}TfO]^{3+}$ peak ($m/z = 1123.36$) of the 1 : 1 **BT4**·HATHCN complex (Fig. S10†).

The UV-vis spectrum **BT4**·HATHCN complex displayed (Fig. 8a) a noticeable decrease in Soret and Q bands intensities (compared to the free **BT4** spectrum) with a concomitant appearance of a characteristic broad CT band (650–870 nm) centered at ~725 nm, indicating ZnTPP/HATHCN π-D/A CT interaction. In addition, in the **BT4**·HATHCN CT complex, the Q bands of ZnTPP (560 and 602 nm) and the longest wavelength absorption of HATHCN (322 nm), which correspond to $S_0 \rightarrow S_1$ transitions, were noticeably blue-shifted (~4–6 nm) compared to the free species, a characteristic sign of face-to-face π-D/A interaction between these two complementary π-systems.[67] In contrast, no UV-vis absorption change of **BT4** was observed in the presence of pyrene (Fig. 8b), indicating the lack of any meaningful electronic interaction between these two electron rich species.

The cyclic voltammetry analysis (Fig. S11†) showed that in the **BT4**·HATHCN complex, the first oxidation (anodic) peak of the ZnTPP core shifted by +40 mV—from +1.14 V for free **BT4** to 1.18 V for the **BT4**·HATHCN CT complex (*vs.* Ag/AgCl in 0.1 M Bu_4N·TfO/CH_2Cl_2 solution)—suggesting that the CT interaction between the electron-rich ZnTPP core and highly π-acidic HATHCN (LUMO: −4.8 eV)[68] made the oxidation of the π-donor harder in the complex. In contrast, no significant shift of the first oxidation (anodic) peak of the ZnTPP core was observed in the presence of electron-rich pyrene due to the lack of such interaction.

Conclusions

In summary, we have demonstrated that Pt(II)-driven social self-assembly of a tetratopic M′TPP ligand and ditopic XDC linkers having different lengths (6.9–11.2 Å) and rigidities yielded novel 2D bow-tie complexes $[\{(Et_3P)_2Pt\}_4(M'TPP)(XDC)_2]\cdot(4TfO)$ featuring a M′TPP core and two parallel XDC linkers that were held together by four heteroligated Pt^{II}(N,O) corners. The most direct and compelling evidence of bow-tie complexes came from the SXRD data, which were fully consistent with their NMR characteristics. The ^{31}P NMR spectra of the resulting tri-component SCCs revealed the formation of heteroleptic Pt^{II}(N,O) corners bearing one carboxylate and one pyridyl group, while the ^{1}H and 2D NMR studies presented telltale signs of bow-tie structures by revealing that the two opposite pyrrole rings carrying the more shielded $H_{c'}$ protons were located inside two isosceles triangles formed by two parallel XDC linkers, while the other two pyrrole rings bearing the less shielded $H_{c''}$ protons remained exposed. The pyridyl arms of M′TPP deviated from their original projections in order to accommodate different XDC linkers having different lengths (~7–11 Å) and rigidities into isosceles triangles. This led to the formation of 2D bow-tie complexes, which were entropically more favored over 3D tetragonal prisms. Thus, these comprehensive studies not only unveiled novel M′TPP-based bow-tie complexes, but also ruled out the corresponding prism formation. These revelations underscore the importance of careful multiprobe characterization and careful data analyses to ensure accurate identification of structures and compositions of SCCs, which is key to proper depiction of their structure–property/function relationships because without accurate characterization in the

first place, we run the risk of misassigning the properties and functions to nonexistent species, as it happened evidently in the case of illusive prisms despite having all the advanced characterization tools and techniques at our disposal. In addition to assembling and accurately characterizing novel bow-tie-shaped tricomponent coordination complexes based on M′TPP ligands, we have demonstrated that these electron-rich species can bind highly π-acidic HATHCN through strong π-D/A CT interaction, but do not interact with π-donors. While the focus of the foregoing studies was to determine the accurate structures and compositions of M′TPP-based tricomponent SCCs and to demonstrate their molecular recognition capability involving π-donor/acceptor interaction, in light of these new revelations it appears that some fascinating properties and functions, such as photodynamic cancer therapy that were previously attributed to M′TPP-based prisms, actually belonged to the corresponding bow-tie complexes. Further studies of potential applications of these bow-tie complexes, such as light-harvesting and energy transduction systems are underway in our laboratory.

Data availability

All relevant experimental and computational data associated with this work have been reported above and in the ESI.†

Author contributions

PAB and MAG conducted most of the experiments, analyzed data, prepared all figures, and helped draft and edit the manuscript; AY helped refine the crystal structures; AJJ performed all ESI-MS analyses; and SS supervised the project, verified data analysis, edited and reviewed the manuscript, and secured funding. All authors read the manuscript and agreed with the content.

Conflicts of interest

The authors declare no conflicts of interest.

Acknowledgements

This work was supported by the National Science Foundation (NSF award no. CHE-1660329 and DMR-1809092) and Clemson University. We also acknowledge the NSF-MRI grant CHE-1725919 for the 500 MHz NMR instrument used for our studies. We thank Dr Colin McMillen for solving the crystal structures of the bow-tie complexes. We also thank the handling editor and the reviewers for strongly encouraging us to emphasize the importance of proper structural characterization of complex supramolecular assemblies for accurate depiction of their structure–function relationships and to highlight how rigorous structural analyses presented here led to rectification of previously mischaracterized tetragonal prisms as bow-tie complexes for the long-term benefit of supramolecular chemistry community.

References

1 M. Fujita, J. Yazaki and K. Ogura, *J. Am. Chem. Soc.*, 1990, **112**, 5645.
2 P. J. Stang and D. H. Cao, *J. Am. Chem. Soc.*, 1994, **116**, 4981.
3 P. J. Stang, B. Olenyuk, J. Fan and A. M. Arif, *Organometallics*, 1996, **15**, 904.
4 P. J. Stang and B. Olenyuk, *Acc. Chem. Res.*, 1997, **30**, 502.
5 A. J. Lees and S.-S. Sun, *Inorg. Chem.*, 2001, **40**, 3154.
6 F. Würthner, C.-C. You and C. R. Saha-Möller, *Chem. Soc. Rev.*, 2004, **33**, 133.
7 N. C. Gianneschi, M. S. Masar III and C. A. Mirkin, *Acc. Chem. Res.*, 2005, **38**, 825.
8 B. H. Northrop, Y.-R. Zheng, K.-W. Chi and P. J. Stang, *Acc. Chem. Res.*, 2009, **42**, 1554.
9 H. T. Chifotides, I. D. Giles and K. R. Dunbar, *J. Am. Chem. Soc.*, 2013, **135**, 3039.
10 M. A. Gordillo, P. A. Benavides and S. Saha, *Cryst. Growth Des.*, 2019, **19**, 6017.
11 K. Kumazawa, K. Biradha, T. Kusukawa, T. Okano and M. Fujita, *Angew. Chem., Int. Ed.*, 2003, **42**, 3909.
12 R. Chakrabarty, P. S. Mukherjee and P. J. Stang, *Chem. Rev.*, 2011, **111**, 6810.
13 T. R. Cook, Y.-R. Zheng and P. J. Stang, *Chem. Rev.*, 2013, **112**, 734.
14 T. R. Cook and P. J. Stang, *Chem. Rev.*, 2015, **115**, 7001.
15 S. Zarra, D. M. Wood, D. A. Roberts and J. R. Nitschke, *Chem. Soc. Rev.*, 2015, **44**, 419.
16 S. Fujii, T. Tada, Y. Komoto, T. Osuga, T. Murase, M. Fujita and M. Kiguchi, *J. Am. Chem. Soc.*, 2015, **137**, 5939.
17 W. M. Bloch and G. H. Clever, *Chem. Commun.*, 2017, **53**, 8506.
18 T. K. Ronson, W. Meng and J. R. Nitschke, *J. Am. Chem. Soc.*, 2017, **139**, 9698.
19 W. Brenner, T. K. Ronson and T. K. Nitschke, *J. Am. Chem. Soc.*, 2017, **139**, 75.
20 S. Saha, I. Regeni and G. H. Clever, *Coord. Chem. Rev.*, 2018, **374**, 1.
21 S. Pullen and G. H. Clever, *Acc. Chem. Res.*, 2018, **51**, 3052.
22 S. Chakraborty and G. R. Newkome, *Chem. Soc. Rev.*, 2018, **47**, 3991.
23 D. Bardhan and D. Chand, *Chem.–Eur. J.*, 2019, **25**, 12241.
24 S. Kitagawa, R. Kitaura and S. Noro, *Angew. Chem., Int. Ed.*, 2004, **43**, 2334.
25 W. L. Leong and J. J. Vittal, *Chem. Rev.*, 2011, **111**, 688.
26 H. Furukawa, K. E. Cordova, M. O'Keeffe and O. M. Yaghi, *Science*, 2013, **341**, 974.
27 K. W. Chi, C. Addicott, A. M. Arif and P. J. Stang, *J. Am. Chem. Soc.*, 2004, **126**, 16569.
28 M. Wang, Y.-R. Zheng, K. Ghosh and P. J. Stang, *J. Am. Chem. Soc.*, 2010, **132**, 6282.
29 Y. R. Zheng, W. J. Lan, M. Wang, T. R. Cook and P. J. Stang, *J. Am. Chem. Soc.*, 2011, **133**, 17045.
30 Y.-R. Zheng, Z. Zhao, M. Wang, K. Ghosh, J. B. Pollock, T. R. Cook and P. J. Stang, *J. Am. Chem. Soc.*, 2010, **132**, 16873.

31 M. Wang, Y.-R. Zheng, T. R. Cook and P. J. Stang, *Inorg. Chem.*, 2011, **50**, 6107.
32 J. B. Pollock, T. R. Cook, G. L. Schneider and P. J. Stang, *Chem.–Asian J.*, 2013, **8**, 2423.
33 Y. Shi, I. Sánchez-Molina, C. Cao, T. R. Cook and P. J. Stang, *Proc. Natl. Acad. Sci. U. S. A.*, 2014, **111**, 9390.
34 Y. Ye, T. R. Cook, S. P. Wang, J. Wu, S. Li and P. J. Stang, *J. Am. Chem. Soc.*, 2015, **137**, 11896.
35 Y. Sun, C. Chen, J. Liu, L. Liu, W. Tuo, H. Zhu, S. Lu, X. Li and P. J. Stang, *J. Am. Chem. Soc.*, 2020, **142**, 17903.
36 G. Yu, T. R. Cook, Y. Li, X. Yan, D. Wu, L. Shao, J. Shen, G. Tang, F. Huang, X. Chen and P. J. Stang, *Proc. Natl. Acad. Sci. U. S. A.*, 2016, **113**, 13720.
37 Z. Li, X. Yan, F. Huang, H. Sepehrpour and P. J. Stang, *Org. Lett.*, 2017, **19**, 5728.
38 M. Zhang, M. L. Saha, M. Wang, Z. Zhou, B. Song, C. Lu, X. Yan, X. Li, F. Huang, S. Yin and P. J. Stang, *J. Am. Chem. Soc.*, 2017, **139**, 5067.
39 G. Yu, S. Yu, M. L. Saha, J. Zhou, T. R. Cook, B. C. Yung, J. Chen, Z. Mao, F. Zhang, Z. Zhou, Y. Liu, L. Shao, S. Wang, C. Gao, F. Huang, P. J. Stang and X. Chen, *Nat. Commun.*, 2018, **9**, 4335.
40 Y. Sun, Y. Yao, H. Wang, W. Fu, C. Chen, M. L. Saha, M. Zhang, S. Datta, Z. Zhou, H. Yu, X. Li and P. J. Stang, *J. Am. Chem. Soc.*, 2018, **140**, 12819.
41 X. Chang, Z. Zhou, C. Shang, G. Wang, Z. Wang, Y. Qi, Z.-Y. Li, H. Wang, L. Cao, X. Li, Y. Fang and P. J. Stang, *J. Am. Chem. Soc.*, 2019, **141**, 1757.
42 X. Chang, Z. Zhou, C. Shang, G. Wang, Z. Wang, Y. Qi, Z. Y. Li, H. Wang, L. Cao, X. Li, Y. Fang and P. J. Stang, *J. Am. Chem. Soc.*, 2019, **141**, 1757.
43 Y. Sun, C. Chen, J. Liu and P. J. Stang, *Chem. Soc. Rev.*, 2020, **49**, 3889.
44 S. Ghosh and P. S. Mukherjee, *Inorg. Chem.*, 2009, **48**, 2605.
45 A. K. Bar, G. Mostafa and P. S. Mukherjee, *Inorg. Chem.*, 2010, **49**, 7647.
46 D. Samanta, S. Shanmugaraju, S. A. Joshi, Y. P. Patil, M. Nethaji and P. S. Mukherjee, *Chem. Commun.*, 2012, **48**, 2298.
47 C. García-Simón, M. Garcia-Borràs, L. Gómez, I. Garcia-Bosch, S. Osuna, M. Swart, J. M. Luis, C. Rovira, M. Almedia, I. Imaz, D. Maspoch, M. Costas and X. Ribas, *Chem.–Eur. J.*, 2013, **19**, 1445.
48 C. García-Simón, M. Garcia-Borràs, L. Gómez, T. Parella, S. Osuna, J. Juanhuix, I. Imaz, D. Maspoch, M. Costas and X. Ribas, *Nat. Commun.*, 2014, **5**, 5557.
49 C. Colomban, G. Szalóki, M. Allain, L. Gómez, S. Goeb, M. Sallé, M. Costas and X. Ribas, *Chem.–Eur. J.*, 2017, **23**, 3016.
50 C. Colomban, V. Martin-Diaconescu, T. Parella, S. Goeb, C. García-Simón, J. Lloret-Fillol, M. Costas and X. Ribas, *Inorg. Chem.*, 2018, **57**, 3529.
51 C. Fuertes-Espinosa, A. Gómez-Torres, R. Morales-Martínez, A. Rodríguez-Fortea, C. García-Simón, F. Gándara, I. Imaz, J. Juanhuix, D. Maspoch, J. M. Poblet, L. Echegoyen and X. Ribas, *Angew. Chem., Int. Ed.*, 2018, **57**, 11294.
52 C. Colomban, C. Fuertes-Espinosa, S. Goeb, M. Sallé, M. Costas, L. Blancafort and X. Ribas, *Chem.–Eur. J.*, 2018, **24**, 4371.
53 C. García-Simón, A. Monferrer, M. Garcia-Borràs, I. Imaz, D. Maspoch, M. Costas and X. Ribas, *Chem. Commun.*, 2019, **55**, 798.
54 V. Vajpayee, S. Bivaud, S. Goeb, V. Croué, M. Allain, B. V. Popp, A. Garci, B. Therrien and M. Sallé, *Organometallics*, 2014, **33**, 1651.
55 E. Ubasart, O. Borodin, C. Fuertes-Espinosa, Y. Xu, C. García-Simón, L. Gómez, J. Juanhuix, F. Gándara, I. Imaz, D. Maspoch, M. Delius and X. Ribas, *Nat. Chem.*, 2021, **13**, 420.
56 G. Yu, Y. Ye, Z. Tong, J. Yang, Z. Li, B. Hua, L. Shao and S. Li, *Macromol. Rapid Commun.*, 2016, **37**, 1540.
57 C. Li, H. Nian, Y. Dong, Y. Li, B. Zhang and L. Cao, *Inorg. Chem.*, 2020, **59**, 5720.
58 Z. Yang, Y. Wang, X. Liu, R. T. Vanderlinden, R. Ni, X. Li and P. J. Stang, *J. Am. Chem. Soc.*, 2020, **142**, 13689.
59 Y. Hou, Z. Zhang, S. Lu, J. Yuan, Q. Zhu, W. P. Chen, S. Ling, X. Li, Y.-Z. Zheng, K. Zhu and M. Zhang, *J. Am. Chem. Soc.*, 2020, **142**, 18763.
60 M. Eddaoudi, J. Kim, N. Rosi, D. Vodak, J. Wachter, M. O'Keeffe and M. Yaghi, *Science*, 2002, **295**, 469.
61 S. Lipstman and I. Goldberg, *Acta Crystallogr., Sect. C: Cryst. Struct. Commun.*, 2009, **65**, 371.
62 L. R. Dinelli, G. Von Poelhsitz, E. E. Castellano, J. Ellena, S. E. Galembeck and A. A. Batista, *Inorg. Chem.*, 2009, **48**, 4692.
63 A. N. Oldacre, M. R. Crawley, A. E. Friedman and T. R. Cook, *Chem.–Eur. J.*, 2018, **24**, 10984.
64 Z. Zhao, Z. Zhang, H. Wang, X. Li and M. Zhang, *Isr. J. Chem.*, 2019, **59**, 299.
65 (*a*) P. Thordarson, *Chem. Soc. Rev.*, 2011, **40**, 1305; (*b*) www.supramolecular.org.
66 T. Aoki, H. Sakai, K. Ohkibo, T. Sakanoue, T. Takenobu, S. Fukizumi and T. Hasobe, *Chem. Sci.*, 2015, **6**, 1498.
67 C. R. Martinez and B. L. Iverson, *Chem. Sci.*, 2012, **3**, 2191.
68 G. Aragay, A. Frontera, V. Lloveras, J. Vidal-Gancedo and P. Ballester, *J. Am. Chem. Soc.*, 2013, **135**, 2620.